

Oedometer tests with measurement of internal friction between oedometer ring and clay specimen

M. R. Lodahl

COWI A/S and Aarhus University, Denmark, mirl@cowi.dk / mirl@eng.au.dk

K. K. Sørensen

Aarhus University, Department of Engineering, Denmark

N. Mortensen

nmGeo, Denmark

H. Trankjær

COWI A/S, Denmark

ABSTRACT

The effects of friction in the oedometer cell have been studied in a series of tests carried out in a cell, where the load transferred to the bottom pressure head is measured, and the friction in the oedometer ring is back-calculated. In the test series, both natural and artificial specimens were tested. Based on these tests, the influence of plasticity of the specimen on the friction and the influence of friction on the stiffness parameters have been assessed. It was found that the friction has insignificant effect on the compression index, whereas swelling and recompression stiffness may be influenced. For the derived tangent stiffnesses, particular when the loading is reversed, an overestimation of up to approx. 30 % was found in the tests due to frictional stress loss.

Keywords: Oedometer test; Friction; High-plasticity clays; Deformation parameters

1 INTRODUCTION

Prediction of the future settlements of structures founded on clay is an important part of the geotechnical design. In many countries, the oedometer test is used for estimating the deformation parameters relevant for the particular design situations. An oedometer cell fulfilling the standards usually has a specific height-to-diameter-ratio to minimize the effects of friction between the oedometer ring and the soil specimen. The minimum diameter-to-height ratio required is 2.5, according to many standards, e.g. ASTM D 2435, BS 1377 - part 5 and DS/CEN ISO/TS 17892-5. Development of friction may affect the results, yielding lower compression, swelling and recompression indices, which in turn may cause unsafe settlement and heave predictions, cf. Watabe et al. (2008).

For Danish Palaeogene, high plasticity clays, a very high stiffness ($E_{oed} \geq 50$ MPa) is

often reported from oedometer tests for the first load step in unloading and reloading after reversal of the loading direction; cf. (Christensen and Hansen 1959; Krogsbøll et al., 2012). The high stiffness identified may be influenced by the friction between the oedometer ring and the tested specimen. Since the direction and magnitude of the frictional stresses are changed when going from loading to unloading and vice versa, the specimen is 'held in place' by the friction, causing the mean stress change for the specimen to be lower than the stress change at top of the specimen, especially for the fixed ring oedometer setup. This effect may thus cause the high reported stiffness for the first step in un- and reloading.

The development of friction between the oedometer ring and the tested specimen may partly be reduced by using a floating ring setup. In the floating ring setup the oedometer ring is unsupported and carried by the fricti-

on. Thus, the total shear force between the specimen and the ring cannot exceed the weight of the ring. However, it should be noted that the magnitude and direction of the shear stresses may vary over the height of the specimen and the stress state is thus unknown.

To investigate the effect of friction on the compression curves obtained from the oedometer cell, a series of tests was planned and carried out. Two natural and four artificial, reconstituted, preconsolidated specimens with known contents of clay minerals were tested using a custom cell (the nmGeo cell) and a cell based on a NGI DSS-membrane, which is essentially friction free.

The overall aim of the study was to investigate the effects of plasticity on the magnitude of the friction between the specimen and the confining ring, and to investigate the effect of a difference in void ratio and hence compressibility of the tested specimen on the magnitude of developed stress loss due to friction.

2 MATERIALS AND METHODS

When a specimen is installed in an oedometer ring, very low friction is initially maintained between the specimen and the oedometer ring, especially when a polished ring coated with vacuum grease is used, which is suggested by most standards, e.g. ASTM D2435. An illustration of the stress state in an oedometer cell is presented in Figure 1 with vertical stress, σ'_v and horizontal stress, σ'_h . As seen from the figure, the frictional shear stress, τ_{ring} , acts upwards during loading and is thus directed downwards during unloading.

The total frictional shear force transferred between the ring and the specimen, F_{ring} is calculated by Eq. (1),

$$F_{ring} = \int_{A_{ring}} \tau_{ring} \quad (1)$$

where A_{ring} denotes the area of the ring in contact with the specimen. In a fixed-ring setup, the stress loss due to friction means that the vertical load changes with depth in the specimen. The magnitude of frictional

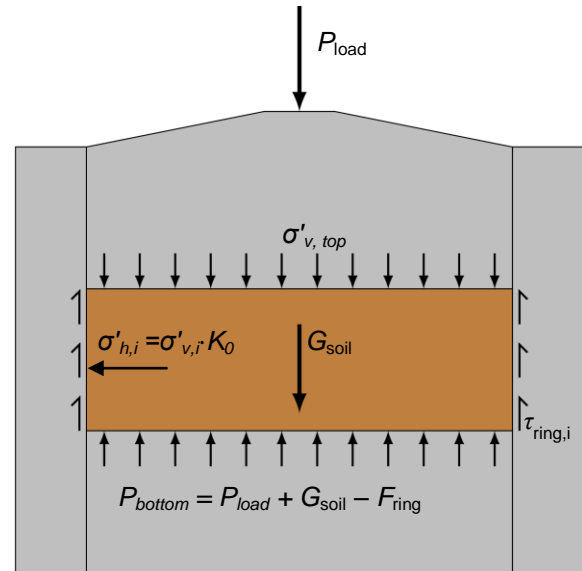


Figure 1: Illustration of stress conditions in the fixed ring oedometer cell (compression stage).

shear stress at end of primary consolidation in depth increment i of the height of the ring, is dependent on the horizontal stress in that depth increment, $\sigma'_{h,i}$, and the interface friction angle, $\delta'_{interface}$, as given in Eq. (2),

$$\tau_{ring,i} = a + K_0 \sigma'_{v,i} \tan(\delta'_{interface}) \quad (2)$$

where a is the adhesion. The coefficient of earth pressure at rest, K_0 , of the tested specimen is typically assumed to be dependent on the angle of internal friction of the soil, ϕ' , and the overconsolidation ratio, OCR , cf. Eq. (3) after Mayne and Kulhawy (1982).

$$K_0 \approx (1 - \sin(\phi')) OCR^{\sin(\phi')} \quad (3)$$

The value of $\delta'_{interface}$ and adhesion may be somewhat lower than the angle of internal friction and effective cohesion of the specimen, e.g. $\delta'_{interface} = 0.5\phi'$ and $a = c'$ was proposed by Lovisa (2014). The dependency of the K_0 -value on OCR suggest that the effect of friction is most significant when the specimen is in an overconsolidated (OC) stress-regime. Thus, the largest values of friction are expected to occur along unloading and reloading curves in oedometer tests due to larger K_0 -values. This claim is supported by the findings of Watabe et al. (2008) in tests on slightly overconsolidated, high plasticity Osaka Bay Clay.

Table 1: Selected classification parameters for the selected core of Little Belt Clay used for testing, cf. Rambøll/Arup JV (2013).

Parameter	Value
Unit weight (kN/m ³)	18.1
e_0 (-)	1.23
Clay fraction (%)	~75
σ'_{pc} (kPa)	400-500*

* Values obtained at similar depth on other specimens extracted from Little Belt, cf. Banedanmark, (2013)

2.1 Natural, undisturbed specimens

The tested natural specimens consist of Little Belt Clay, sampled in Little Belt, Denmark. A borehole with full retrieval of cores were drilled approx. 50 m from the first pier on the Funen side of the Little Belt Bridge from 1935. A Geobor-S system with a triple barrel coring device was employed to retrieve the undisturbed cores which were wrapped in cling film and waxed inside a cardboard pipe before storage. Both natural specimens reported in this study origins from borehole 10.A.801, core no. 10-107904, sampled from a depth of 18.0 – 18.6 m below the seabed. The sampled Little Belt Clay is a marine sedimentary, Palaeogene clay and is described as a slightly fissured clay of very high plasticity, slightly calcareous. Selected classification parameters for the core of Little Belt Clay are presented in Table 1.

Two specimens of intact Little Belt Clay (LB001 and LB002) were hand-trimmed to fit the applied oedometer devices. Water content, w , initial void ratios, e_0 and degrees of saturation prior to testing, S_0 are presented in Table 2, along with index parameters, w_L , w_p and I_p determined from the trimmings. The diameter of the tested specimens in the special cell were 60 mm and the height approximately 20 mm, whereas the diameter of the specimens tested in the DSS-membrane cell are 66.8 mm and the specimen height approximately 20 mm.

2.2 Artificial, reconstituted specimens

To analyse the effect of the mineralogical composition of the clay on the magnitude of the developed friction, four tests were carried out using artificial, reconstituted, pre-consolidated clay specimens.

Table 2: Classification parameters and natural water content for the tested specimens.

	w_p (%)	w_L (%)	I_p (%)	w (%)	e_0 (-)	S_0 (%)
LB001	44	182	138	42	1.15	98
LB002	41	180	138	41	1.06	100
K60B40 (x2)	37	177	140	84	2.23- 2.45	95- 99
K100B0 (x2)	32	59	27	42	1.14- 1.16	95- 97

The clay specimens were prepared from bentonite and kaolinite powders, mixed in different ratios. In the present paper, the specimens are named after the convention KXXBYY, where the XX signifies the percentage of kaolinite and YY the percentage of bentonite, both determined from dry mass.

The clay powders were mixed with tap water to form a slurry with a water content $w = 1.25w_L$, cf. Burland (1990). The slurry was then installed in Ø70 mm acrylic floating ring consolidometers and preloaded incrementally to a final nominal stress of 163 kPa. The final height of the preconsolidated slurries were sufficient to allow two specimens to be trimmed; one for each oedometer cell. Frictional effects may have developed between the sample and the acrylic tube wall, which may have lowered the actual preconsolidation pressure. However, measures as applying a thin coating of vacuum grease inside the cylinder prior to installation of slurry and moving of the acrylic ring between the load steps were taken to avoid excessive build-up. The classification parameters and water contents for the specimens in the present study are presented in Table 2.

2.3 Oedometer apparatus

An oedometer cell able to measure the accumulated friction between the oedometer ring and the test specimen was developed by nmGeo. This oedometer cell, the nmGeo-cell, is a further development of the oedometer cells developed by Moust Jacobsen, cf. Jacobsen (1970). The cell consists of a very rigid steel ring, a bottom plate, a lower pressure head and an upper pressure head. A force transducer was fitted between the bottom plate and the bottom pressure head, enabling measurements of the force transferred to the bottom pressure head by the soil specimen.

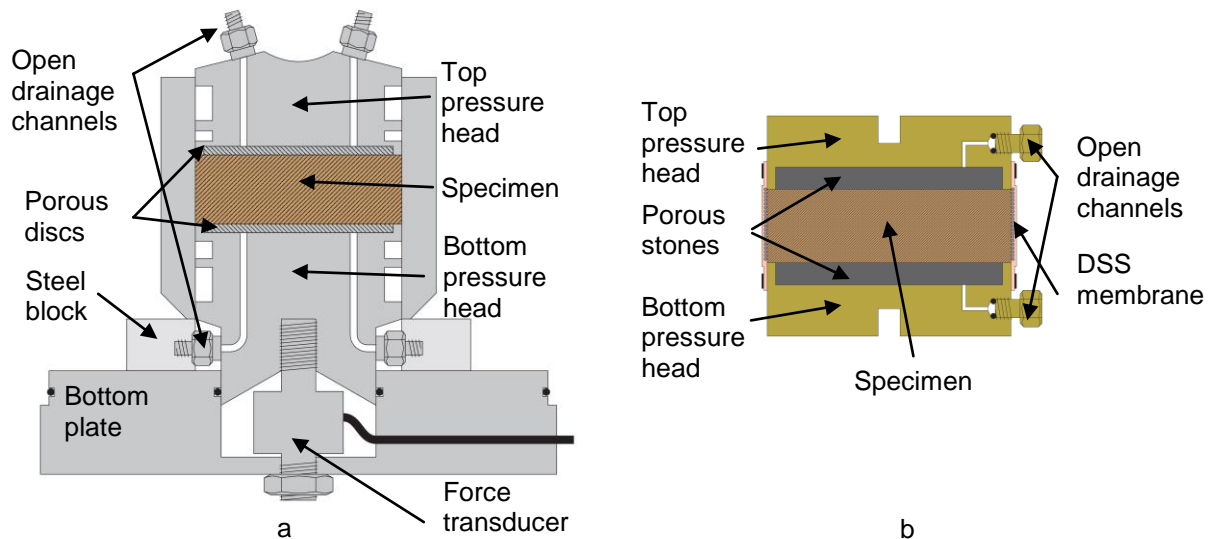


Figure 2: Illustration of the oedometer cells used in the tests presented in this paper. a) the nmGeo-cell and b) the NGI DSS-membrane cell.

Steel blocks and a yoke support the ring to prevent movement of the ring in loading and unloading, respectively, creating a fixed-ring setup. Thus, any difference in the applied total force and the force measured by the force transducer between the bottom plate and the bottom pressure head is caused by frictional loss. A sketch of the nmGeo-cell is presented in Figure 2a.

A NGI DSS membrane cell was used in parallel with the nmGeo-cell (cf. Figure 2b), to obtain results which are almost unaffected by friction between specimen and oedometer ring. In the DSS-cell setup, the 'oedometer ring' consists of a steel-reinforced rubber membrane, which prevents radial expansion of the specimen, but allows axial deformation, cf. NGI (2015). As only vertical loading was applied in the tests, porous stones without spikes were applied.

All oedometer tests were performed as incrementally loaded (IL), 1D compression tests without pore pressure measurements, using double-sided drainage. The Geocomp LoadTrac III loading frame was used during the tests, where the applied load was controlled by a stepper motor based on readings from a S-type load cell. The axial strain was measured by a potentiometric displacement transducer and was corrected for self-deflection of the loading frame measured on a rigid steel disk using the planned load steps. For

Table 3: Concentration of the artificial pore water PC02 used for testing of natural specimens, cf. Rambøll Arup Joint Venture, (2014) and tap water used for artificial specimens, cf. Aarhus Vand A/S, (2015).

Ion	Concentration [mg/l]	
	PC02 water	Tap water
Cl ⁻	13500	29
SO ₄ ⁻	545	48
Na ⁺	8030	26
K ⁺	82	3.3
Mg ⁺⁺	235	11
Ca ⁺⁺	405	96

the nmGeo cell, simultaneous readings of the displacement and the load transferred to the bottom pressure head were recorded during the tests.

2.4 Test methods

The specimens were loaded incrementally, allowing for full consolidation prior to application of the next load step, avoiding excessively long phases of secondary consolidation. The specimens were installed in the oedometer cells and a seating pressure was applied before the cell water was added during the first load step. No volume change was allowed during the first load step. For the natural specimens the Fehmarn Belt artificial pore water PC02 was used to simulate natural pore water conditions for the specimen, whereas the artificial specimens were tested

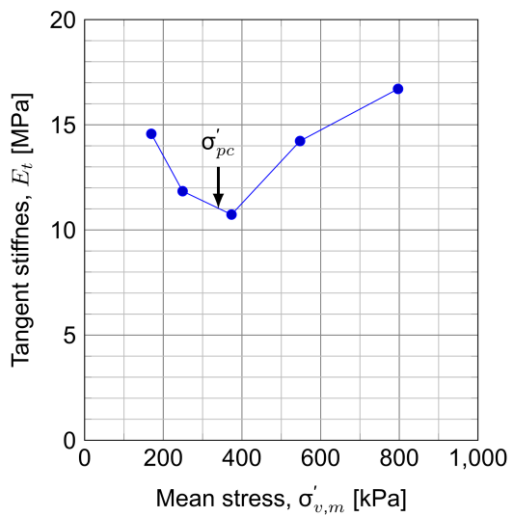


Figure 3: Janbu plot for specimen LB002 with interpreted preconsolidation pressure along the initial loading curve.

using tap water. The ion-concentration of the pore fluids is presented in Table 3.

Due to limitations in the capacity of the DSS-membrane, the maximum load applied to the specimens were limited to 1100 kPa. A load increment ratio of 1.5 was adopted to achieve a closer spacing of the load steps, meaning that the load in a new load step was increased with half of the total load from the previous load step. In unloading the same load steps were applied as in loading. However, during unloading every other load step was skipped for the sake of time as each of the load steps took up to 48 hours to achieve complete consolidation. The obtained time-

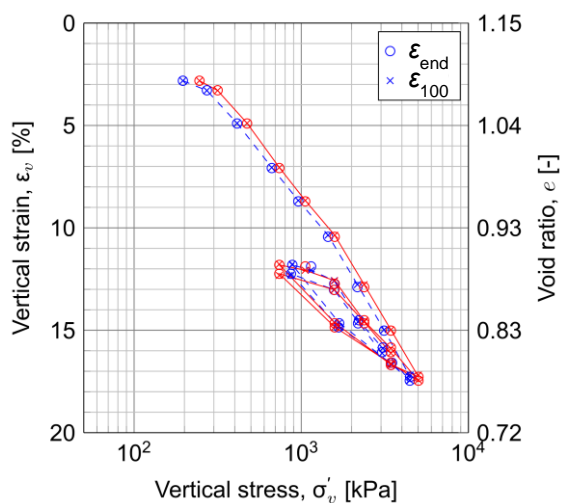


Figure 4: Stress-strain curve for specimen LB001 obtained using the nmGeo-cell. Red line denotes the stress at the top pressure head, whereas the dashed blue lines denotes the stress calculated from the force measured in the bottom plate.

settlement curves were interpreted using the Casagrandes method, Casagrande (1938). The stress-strain curves were analysed using the theory of both Casagrande (1936) and Janbu (1969) to identify the apparent pre-consolidation pressure, σ'_{pc} , cf. Figure 3.

3 RESULTS

The obtained results from the natural specimens are presented in section 3.1, and results from reconstituted, artificial specimens are presented in section 3.2.

3.1 Natural, undisturbed specimens

The specimens, LB001 and LB002 were tested using the nmGeo-cell and the DSS-membrane, respectively. The obtained stress-strain curves are presented in Figure 4 and Figure 5, respectively. As seen from the figures, the maximum obtained stress levels were very different, which was mainly due to the limitation of the DSS membrane. In Figure 4 two stress-strain curves are presented; one linking strains with the applied loading at the top pressure head (as usually done) and one using the measured force below the bottom pressure head. Both stress readings were plotted with the same measured axial strain. As seen from the figure, an offset is present between the two curves, illustrating the magnitude of friction developed during testing. As seen from Figure 4 the points plotted using the measured values of the stress at the bottom

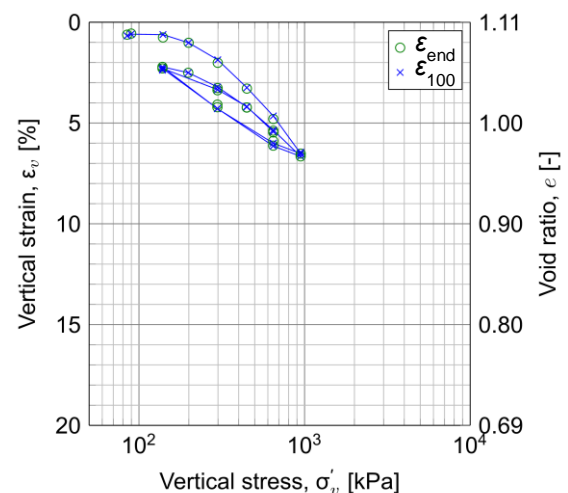


Figure 5: Stress-strain curve for specimen LB002 tested with the DSS-membrane cell.

Table 4: Stiffness parameters determined for tests on intact Little Belt Clay and on artificial mixtures.

Parameter	LB001 nmGeo	LB002 DSS	K100B0		K60B40		Stress range (σ'_v)
			DSS	nmGeo*	DSS	nmGeo	
C_C [-]	0.25	0.26	0.32	0.45	1.35	1.30	LB001: 300 – 5000 kPa LB002: 300 – 950 kPa Artificial: 150 – 1000 kPa
C_S [-]	0.15	0.14	0.05	0.08	0.33	0.25	LB001: 5000 – 750 kPa LB002: 950 – 140 kPa Artificial: 700 – 70 kPa
C_R [-]	0.18	0.16	0.07	0.09	0.47	0.29	LB001: 1050 – 5000 kPa LB002: 200 – 950 kPa Artificial: 100 – 700 kPa

* Significant soil loss observed after testing.

pressure head plotted to the left of the points plotted with the values of applied loading and vice versa when in unloading, i.e. the direction of the friction is as stated in section 2.

The stiffness parameters determined from the oedometer tests are presented in Table 4 and preconsolidation pressures in Table 5.

The obtained C_C values are in the lower range compared to values obtained by Sørensen and Okkels (2015), who suggested $C_C = 0.25 - 0.65$ for $I_p = 140\%$ based on $\sigma'_v \geq 5000$ kPa, which was expected due the lower stress levels applied in the current tests.

3.2 Artificial, reconstituted specimens

The obtained stress-strain curves for the artificial specimens are presented in Figure 6 to Figure 9. The K60B40 specimens had same plasticity index, I_p as the natural Little Belt clay, cf. Table 2. However, the obtained com-

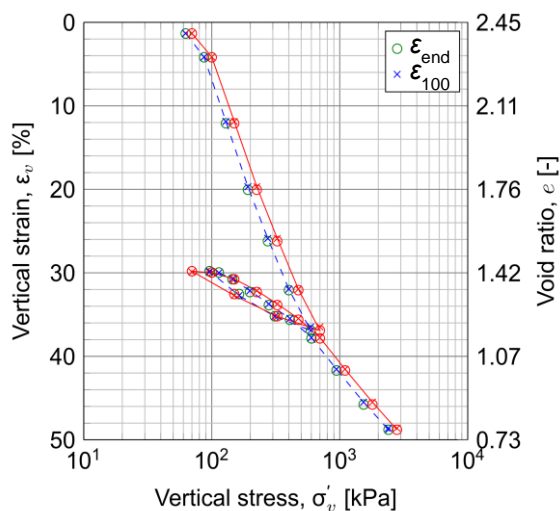


Figure 6: Stress-strain curve for a K60B40 specimen tested in the nmGeo cell. Red line denotes the stress at the top of the specimen, and dashed blue lines the stress at bottom of the specimen.

pression indices were larger for reconstituted specimens compared to natural specimens which may be have been due to differences in structure, pore fluid salinity, etc.

As seen from the stress-strain curves obtained with the nmGeo-cell (Figures 6 and 8), the friction acted in the opposite direction of the load change as for intact specimens, except for first step in unloading and reloading. The derived stiffness parameters are presented in Table 4 and σ'_{pc} -values in Table 5.

4 DISCUSSION

The friction acted in the opposite direction of the applied load increment, which is why the stress at the bottom pressure head was small when the specimen was in loading and vice versa when in unloading. In the individual tests, the difference between the top and the bottom stress (in %) was rather constant on the primary compression curve (e.g. Figure

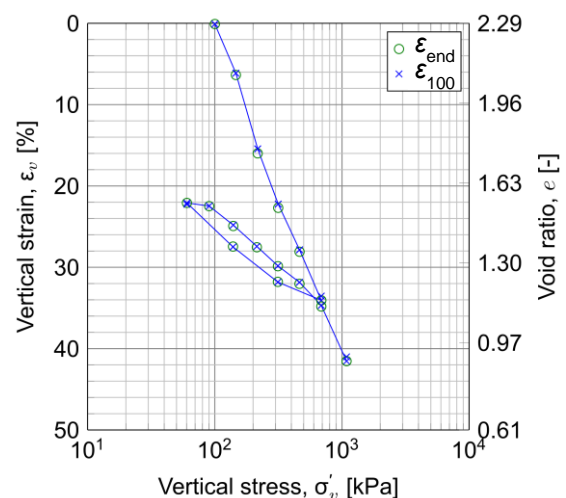


Figure 7: Stress-strain curve for a K60B40 specimen tested in the DSS-membrane cell.

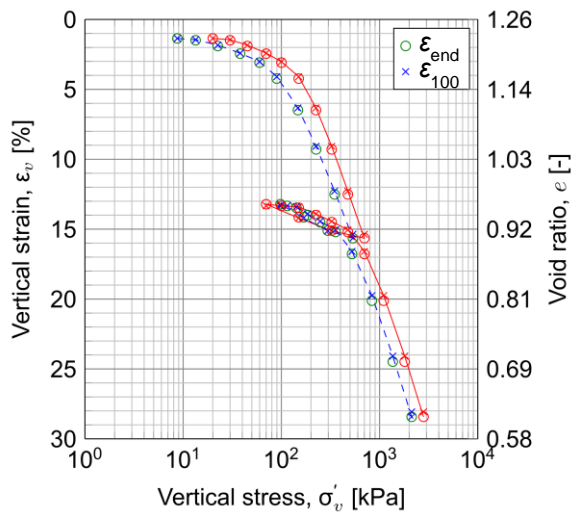


Figure 8: Stress-strain curve for a K100B0 specimen tested in the nmGeo cell. Red line denotes the stress at the top of the specimen, and dashed blue lines the stress at bottom of the specimen.

8), which is why practically no influence was seen on the compression indices obtained using the nmGeo cell and the NGI DSS cell, cf. Table 4.

However, when the loading was reversed, the actual stress change was smaller than expected, which is why the swelling and recompression index identified for the first load steps when reversing the load direction may be very wrong. For all the tests performed in the nmGeo-cell, the loss (in %) of vertical stress due to friction between the specimen and the oedometer ring is plotted against the

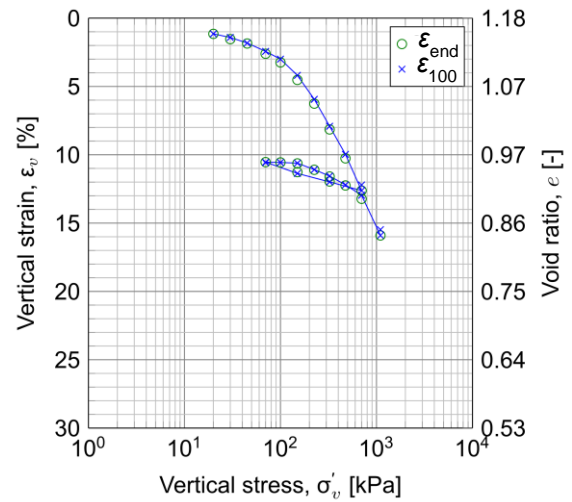


Figure 9: Stress-strain curve for a K100B0 specimen tested in the DSS-membrane cell.

applied stress, cf. Figure 10. As seen from the figure, the stress loss due to friction was rather constant (in %) for normally consolidated (NC) load steps, as may also be inferred from the compression curves. The curve in Figure 10 for the specimen of pure kaolinite K100B0, suggests a very large friction during initial loading, which may be linked with the observed loss of soil during testing (liquefied soil residue was found on top of the upper pressure head after testing. This residue had been squeezed out between the ring and the upper pressure head). Generally, when in unloading, the friction increased and hence the stress loss increased for all specimens. As

Table 5: Apparent preconsolidation pressures σ'_{pc} determined for tests on intact Little Belt Clay and on artificial mixtures. For the nmGeo cell (T) designates measurement from top pressure head and (B) bottom pressure head.

Stage	Parameter	LB001 nmGeo	LB002 DSS	K100B0		K60B40	
				DSS	nmGeo	DSS	nmGeo
Initial loading	σ'_{pc} [kPa] Casagrande	*	260	150	190 (T) 130 (B)	~100	70 (T) 80 (B)
	σ'_{pc} [kPa] Janbu	*	340	140	180 (T) 110 (B)	~150	110 (T) 100 (B)
	Past σ'_{max} [kPa]	>3000 (geological)		163 (preconsolidation of slurry)			
1. reloading	σ'_{pc} [kPa] Casagrande	1660 (T) 1490 (B)	325	570	700 (T) 490 (B)	130	270 (T) 350 (B)
	σ'_{pc} [kPa] Janbu	1700 (T) 1550 (B)	365	280 [†]	670 (T) 440 (B)	130	190 (T) 160 (B)
	Past $\sigma'_{max,lab}$ [kPa]	5020 (T) 4480 (B)	946	694	700 (T) 534 (B)	688	700 (T) 593 (B)

[†] Not identified due to lack of load steps below σ'_{pc} .

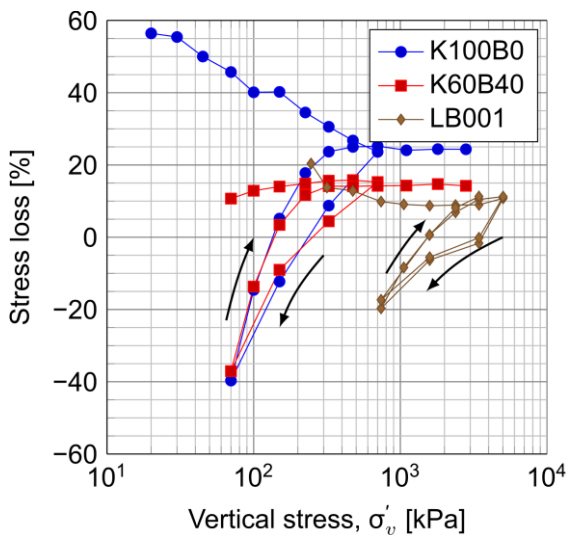


Figure 10: Illustration of stress loss during testing for all specimens tested in the nmGeo cell.

seen from Figure 10 a maximum of 20 % and 40 % stress loss was obtained for the natural and artificial specimens, respectively, for the final unloading step.

4.1 Natural vs. reconstituted specimens

Comparing the tests on natural, intact Little Belt clay with the tests on artificial, reconstituted K60B40, a large difference in compression potentials was seen, even as both specimens had the same plasticity index, I_p , cf. Figure 4 and Figure 5 versus Figure 6 and Figure 7. This was expected as the artificial specimens lacked the natural structure found in the intact clays. As seen from Table 4, the effect the natural structure on the compression index was rather significant. However, no significant difference on the magnitude of measured friction in NC range was found in the tests, when results from LB001 and K60B40 were compared, cf. Figure 10. However, it is unknown whether the difference in stress loss for the final load step in unloading was observed due to the difference in the initial structure of the specimens.

4.2 Influence of plasticity

As seen from Figure 10 the stress loss (in %) for the NC load steps in the stress-strain curves tended to be constant, yielding an unique value for the individual specimens. As seen from the figure, the specimen of pure kaolinite (K100B0) yielded higher stress loss (≈ 25 % loss in the NC regime) compared to speci-

Table 5: Calculated and measured stress loss in NC and OC stress regime using $a = 0$ kPa.

	NC		OC*	
	Calc. †	Meas.	Calc. †	Meas.
K100B0	14 %	24 %	40 %	39 %
K60B40	9 %	14 %	20 %	37 %
LB001	14 %	10 %	23 %	20 %

* $OCR = 10$ for artificial specimens and $OCR = 6.8$ for Little Belt specimen.

† Actual height of the specimen during testing is used for calculating contact area of ring and soil.

mens of higher plasticity (K60B04 and LB-001) where 10 – 15 % loss was identified. This effect may be explained from a lower angle of internal friction for the high plasticity specimens. Generally a decreasing angle of internal friction, ϕ' has been reported with increasing plasticity, e.g. by Sørensen and Okkels (2013) for Palaeogene clays of high plasticity ($I_p \geq 50$ %), incl. Little Belt Clay. From a low ϕ' follows a low $\delta'_{interface}$ between the oedometer ring and the soil specimen, which in turn limits the magnitude of stress transfer (even as K_0 increases). ϕ'_{peak} was found to be approximately 26° for kaolinite cf. Terzaghi et al. (1996), and a $\phi'_{peak} \approx 17^\circ$ may be calculated from Eq. 6 in Sørensen and Okkels (2013) for Little Belt clay and K60B40.

From Eq. (1) - (3) the expected stress loss due to friction was calculated based on the ϕ' suggested above for the specimens. A comparison of the measured and the calculated stress loss due to friction is presented in Table 5. As seen from the table the calculated loss for NC conditions was much lower than what was observed in the K100B0 test, whereas the values for OC conditions were very close. For the K60B40 specimen, the calculated value for NC conditions was quite close to what was measured during the test, whereas the value for OC conditions was much below the measured value. For the Little Belt Clay both calculated values were in good correspondence with what was observed in the tests. Using the actual adhesion of the tested specimens, may introduce a better correspondence between the calculated and the observed results. However, as a was unknown for the specimens, $a = 0$ kPa was assumed in the presented calculations.

For $OCR \geq 1$ no plateau was identified in any tests as seen for the NC regime, cf.

Figure 10. However, it remains unknown whether the observed development of the frictional stress loss was due to the reversal of direction of the shear stresses between specimen and ring, or the change in K_0 during loading. Possibly both effects were at play.

4.3 Determination of oedometer stiffness

As the stress loss from friction influenced the obtained mean stress subjected to the tested specimens, the oedometer modulus that can be calculated from the oedometer test was affected. In Figure 11 the calculated oedometer stiffness, E_{oed} for specimen K60B40 is presented for the reloading phase. E_{oed} was calculated based on the stress at the top of the specimen, σ'_{top} and on the average value of the stress at the top and the bottom of the specimen, σ'_{avg} . σ'_{avg} was expected to be the closest representation of the actual behaviour of the tested specimen. As seen from the figure, the influence of the stress loss on the measured stiffness was most radical in the beginning of the reloading phase where a 26 % too large E_{oed} was calculated, if σ'_{top} was used as reference, whereas the error was smaller for the rest of the load steps. For the final three load steps E_{oed} increased linearly with σ'_v as known from Janbus (1969) framework. The modulus number, m , seemed not to be influenced by the frictional stress loss.

For the specimens K100B0 and LB001, the same tendencies were observed; a clear overestimation of E_{oed} (28 % for K100B0 and 10 % for LB001) in the first reloading step and a similar m calculated from σ'_{top} and σ'_{avg} for the final NC load steps. As may be observed from Figure 11, the friction affected both the stiffness and the applied stresses and hence both values should be corrected. However, from all the tests a high initial stiffness was identified for the first step in reloading.

4.4 Preconsolidation pressure in reloading

An interesting characteristic of both the Little Belt Clay and the K60B40 specimens is the low σ'_{pc} identified along the recompression curve from the test, despite having been subjected to a much higher stress level, cf. Figures 4 and 6 and Table 5. This effect has been presented as a 'lack of stress memory' of

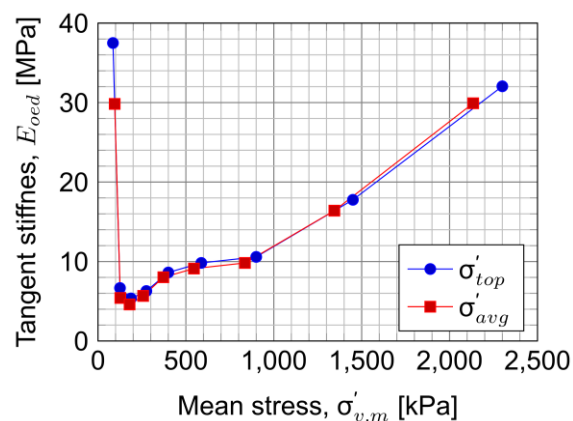


Figure 11: Calculated oedometer stiffness, E_{oed} for specimen K60B40.

the Danish Palaeogene clays cf. (Krogsbøll et al., 2012 and Mortensen, 2012). As this effect was found for the specimens with the highest content of smectite and thus the highest plasticity (Little Belt Clay and K60B40), it may be assumed that the high content of smectite in the natural Palaeogene clays is responsible for this observed behaviour. The content of smectite may thus be the cause of the gradual yield as suggested by Lodahl and Sørensen (2015).

4.5 Limitations of conducted tests

The behaviour of the tested specimen will depend on a stress level located between the applied load and measured load. However, as the distribution of the frictional forces was not known over the height of the ring, the exact value cannot be found. A simple mean value has been used in the present paper which was expected to be sufficiently accurate.

5 CONCLUSION

The tests presented in this paper focused on the development of interface friction between the oedometer ring and the test specimen for a fixed-ring setup. Three specimens were tested in the nmGeo cell, where the stress lost due to friction were measured below the lower pressure head, and three in the NGI DSS-membrane cell, which is essentially friction free due to the ability of the membrane to deform. The stress loss observed in the tests was compared with theoretical estimations for NC and OC conditions.

From the conducted oedometer tests a constant stress loss due to friction (in %) was observed for NC load steps. Thus, the effect on the deformation parameter, C_C , was small due to the logarithmic stress axis. However, when assessing the recompression index, C_R the effect of friction caused the apparent stiffness to be too large, as the unloading stress sustained by the specimen was larger than the top stress (up to 40 % loss). Calculating E_{oed} for first reloading step yielded an overestimation of 26 – 28 % for artificial specimens and 10 % for the natural specimen. Thus, the frictional effects may cause excessively high stiffness if not accounted for. However, it should be kept in mind that the applied stress was underestimated for the first load steps on the recompression branch.

An effect of the plasticity was found in the tests, where specimens of lower plasticity yielded higher frictional losses compared to the specimens of higher plasticity. This effect may be explained by the lower angle of internal friction of the high plasticity specimens. The lower angle of internal friction causes a lower $\delta'_{interface}$ -value and thus lower interface friction even as K_0 increases.

6 ACKNOWLEDGEMENTS

Banedanmark is acknowledged for allowing the use of the intact samples from Little Belt.

A series of preliminary tests were performed at NGI, Oslo using both the nmGeo cell and the DSS-membrane cell. The first author is very grateful for valuable advices and the fruitful environment during his stay in the lab at NGI. The willingness of NGI to share experience, help and equipment is greatly appreciated.

The technical director of nmGeo is acknowledged for lending the nmGeo-cell to be used in the present research.

All conclusions presented in this paper is the responsibility of the authors and does not necessarily reflect the opinions of the bodies mentioned above.

7 REFERENCES

- Aarhus Vand (2015). Bederværket, Udvidet control, personal correspondence.
- Banedanmark (2013). Stability of the Bridge Piers of the Little Belt Bridge – Cover Report on the Work of the Geotechnical Expert Panel.
- Burland, J.B. (1990). On the compressibility and shear strength of natural clays, *Géotechnique* 40(3), 329-378. DOI: 10.1680/geot.1990.40.3.329.
- Casagrande, A. (1936). Determination of the pre-consolidation load and its practical significance. 1st ICSMFE, 3(D-34), 60-64.
- Casagrande, A. (1938). Notes on Soil Mechanics – First Semester" Harvard University (unpublished), Cambridge MA. As cited by (Holtz et al, 2011).
- Christensen, N.H. & Hansen, B. (1959). Shear strength properties of Skive septarian clay. DGI bulletin No. 7.
- Holtz, R.D., Kovacs, W.D. & Sheahan, T.C. (2011). Introduction to Geotechnical Engineering, Pearson, ISBN: 9780137011322.
- Jacobsen, M. (1970). New oedometer and new tri-axial apparatus for firm soils. DGI bulletin No. 27.
- Janbu, N. (1969). The resistance concept applied to deformations of soils. Proc. 7th ICSMFE, 191-196.
- Krogsbøll, A., Hededal, O. & Foged, N. (2012). Deformation properties of highly plastic fissured Palaeogene clay – Lack of stress memory? 16th NGM (DGF-Bulletin 27), 133-140.
- Lodahl, M.R. and Sørensen, K.K. (2015). Influence of smectite content on the one-dimensional deformation behaviour of reconstituted high plasticity clays, 6th ISDCG, Argentina, 1057-1064. DOI: 10.3233/978-1-61499-601-9-1057
- Lovisa, J. and Sivakugan, N. (2014). Tall Oedometer testing: Method to account for Wall Friction. International Journal of Geomechanics, 15(2), DOI: 10.1061/(ASCE)GM.1943-5622.0000359.
- Mayne, P.W. and Kulhawy, F.H. (1982). K_0 -OCR relationships in soil. J. Geotech. Eng. Div. ASCE, GT6, 851-872
- Mortensen, N. (2012). High plasticity Palaeogene clay; A soil type with a very moderate long-term memory. 16th NGM (DGF-Bulletin 27), 413-420.
- NGI (2015). Direct simple shear test – DSS. <http://www.kortlink.dk/ngi/kcpc> (Accessed 30.10.15)
- Rambøll Arup Joint Venture (2014). Ground investigation report. Volume 1 and 2 of 2. Femern-doc GDR 00.1-001, 2013.
- Sørensen, K.K. and Okkels, N. (2015). Correlations between compression index and index parameters for high plasticity Palaeogene clays. 16th ECSMGE. 3371-3376.
- Sørensen, K.K. and Okkels, N. (2013). Correlations between drained shear strength and plasticity index of undisturbed overconsolidated clays. 18th ICSMGE, 423-428.
- Terzaghi, K., Peck, R.B. & Mesri, G. (1996). Soil Mechanics in Engineering Practice. Third Edition. John Wiley & Sons. ISBN 9780471086581.
- Watabe Y., Udaka, K., Kobayashi, M., Tabata, T. & Emura, T. (2008). Effects of friction and thickness on long-term consolidation behaviour of Osaka bay clays. Soils and Foundations, 48(4), 547-561.